Sensors and Actuators B 234 (2016) 412–419

Contents lists available at ScienceDirect

Sensors and Actuators B: Chemical

journal homepage: www.elsevier.com/locate/snb

Determining biosensing modes in SH-SAW device using 3D finite element analysis

Jennifer Brookes[a,*], Rory Bufacchi[a], Jun Kondoh[b], Dorothy M. Duffy[a,c], Rachel A. McKendry[a,d]

[a] London Centre for Nanotechnology, University College London, UK
[b] Graduate School of Science and Technology, Shizouka University, Hamamatsu 432-8561, Japan
[c] Physics & Astronomy, University College London, UK
[d] Division of Medicine, University College London, UK

ARTICLE INFO

Article history:
Received 16 September 2015
Received in revised form 18 March 2016
Accepted 21 March 2016
Available online 6 May 2016

Keywords:
Shear horizontal surface acoustic waves (SH-SAW)
Guiding layer
Finite element analysis (FEA)
Point of Care (POC)

ABSTRACT

Surface acoustic wave (SAW) sensors are electromechanical devices that exploit the piezoelectric effect to induce elastic (acoustic) waves which are sensitive to small perturbations: for example specific binding and recognition of disease biomarkers. Shear horizontal surface acoustic waves (SH-SAWs) are particularly suited to biosample analysis as the wave is not completely radiated and lost into the liquid medium (e.g., blood, saliva) as is the case, for example, in a device implementing Rayleigh waves. Here, using 3D finite element analysis (FEA) the nature of waves launched on a particular quartz device is investigated with respect to the cut of the quartz, the addition of gold guiding layers, and the addition of other linear elastic materials of contrasting acoustic properties. It is demonstrated that 3D FEA analysis showing the device's frequency shift with added guiding layer height reveals a proportional relationship in agreement with the Sauerbrey equation from perturbation theory. It is directly shown, given certain device parameters and a gold guiding layer, that shear horizontally polarized waves are launched on the surface with a dominant mode frequency around 250 MHz. This would be an appropriate biosensing mode in Point of Care (POC) testing for the particular properties of certain disease biomarkers delivered via a liquid medium.

1. Introduction

Surface acoustic wave (SAW) sensors show significant promise for Point of Care sensors with the ability to detect ng-pg/ml biomarkers (e.g., virus, bacteria, hormone), within minutes in a handheld format [1], see Fig. 1. SAWs are ubiquitous, they are used in mobile phone technology, thus they are affordable and readily available, and amenable to integration into POC early warning systems. For example, a mobile phone connected diagnostic device using SAW sensor chips can be developed to diagnose infections, and then immediately transmit results into healthcare systems with geolocated information.

The development of SAW sensors with accurate and specific disease diagnosis is an exciting prospect for biosensors in global healthcare and understanding the surface chemistry and sensor operation is essential for such development. Though the signal transduction in SAWs has been established and quantified for some materials applied to the sensor, the mechanism of signal transduction induced by biomolecules is yet to be fully established. Research conducted based on the Campbell and Jones method [2], has helped to significantly improve our understanding of the role of mass, viscosity, density, shear modulus, conductivity and permittivity changes that occur on a sensor surface and how these changes translate into the SAW response. However this has been with particular onus on the lithium tantalate SAW, which is now well characterized for sensor response [3,4].

The aim of this article is to demonstrate that finite element analysis, FEA, is a very useful mathematical tool for investigating the nature of shear horizontal surface acoustic waves (SH-SAWs). These waves are shown to be launched on a quartz device coated with a gold layer that guides the wave, and demonstrates an effect that is corroborated by previous theory, thus we provide a model platform that can be used reliably in general device design. These types of acoustic waves, SH-SAWs, are particularly suited to detection of biological specimens; concentrating the energy of the wave into the surface increases sensitivity of the sample, and the polarization

* Corresponding author.
E-mail address: j.brookes@ucl.ac.uk (J. Brookes).

http://dx.doi.org/10.1016/j.snb.2016.03.103

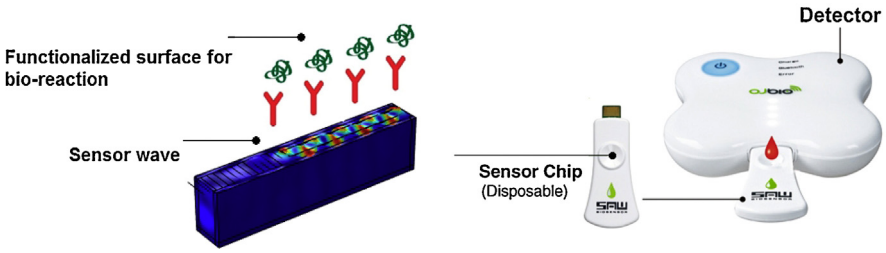

Fig. 1. Figure to demonstrate the SAW sensor chip as integrated into a mobile detector to diagnose infections, as developed by OJBIO. Adapted from [1].

of the wave enables it to propagate effectively within liquid. One important advantage of FEA as a tool for this analysis is that a 3 dimensional model can be easily generalized for various configurations to enable sensors of different materials, and various types of biolayers to be evaluated, quickly and easily, once a basis model has been verified. Further, examining the device in 3D evades the assumption of a pure SH-SAW (displacements solely in one direction) so that the investigation of device sensitivity to parameters such as cut and geometry can be fully explored. Thus, this research describes a "baseline" model of the SH-SAW quartz device, that is known to effectively detect disease.

1.1. SH-SAWS

The particular type of acoustic wave examined in our model is a SH-SAW. SH-SAWs are characterized by displacements in the plane of the surface and a compressional component which is along the direction of propagation. The SH-SAW has an advantage in biological applications because there is virtually no acoustic loss in water which is likely to be the medium in which the sample will be deposited in POC. In the SAW device investigated here interdigitated transducer fingers (IDTs) are the source of an alternating voltage that launches the mechanical wave on the surface of the sensor via the *indirect* piezoelectric effect. This is initiated at the transmitting IDT's, whilst past the sensor distance L, at the receiving IDT's, the wave is converted back to a voltage/current, via the *direct* piezoelectric effect. When the wave travels with no disturbance this is the baseline signal, but when the wave is perturbed by a biomarker on the sensor surface, a change in signal is monitored. The changes in signal that are read and plotted against time, changes in phase $\Delta\varphi$ and amplitude ΔA for example, give information about the sample probed in real time. It is of great theoretical and experimental importance to quantify and determine exactly the perturbative effects inflicted on this particular wave in order to aid the design of sensors, for very particular and sensitive disease diagnosis in biosamples. Towards this goal we investigate the nature of the SAW baseline signal. Understanding and refining the model of the device before perturbation is necessary before it is possible to determine the effect of these biolayers, so the focus of this article is on the robust characterization of the device.

The main determinants of the type of waves elicited by a SAW device are (i) the piezoelectric material of the device, (ii) the cut and therefore the wave propagation type and (iii) the periodicity of the IDT fingers [5]. SAW propagation is not identical in all directions, but anisotropic, so we look for a dominant wave that can encode information optimally as it travels from the input IDT to the output IDT. The device parameters modelled in this instance are: an operating frequency of 250 MHz and an acoustic wavelength of 20 μm, over the acoustic path length (9 mm) there is a time delay of 1.8 μs. The device is made from 36-degree Y-cut quartz substrates (or "36Y-90X quartz") which, as mentioned, largely determines the launched wave characteristics displayed in the results, Section 3. Given these device parameters it is predicted that the waves generated will be surface skimming bulk waves (SSBWS) or shear horizontal bulk waves [5]. An energy trapping layer can theoretically convert these waves into Surface Transverse Waves (STWs), or "guided" or "Love" waves, depending on the degree of energy trapping. The STW is typically caused by an added corrugated surface and the guided or Love wave is caused by a thin continuous layer [6]. We examine the latter with FEA. In this particular case the guided wave demonstrates shear horizontal components (SH-SAW). The principle in the "guiding" is that the added layer, of a lower acoustic velocity than that of the device, concentrates the energy of the wave onto the surface, as opposed to getting dissipated into the bulk of the device, thus rendering the device more sensitive to the surface perturbations. This is exactly what we observe here under the application of a gold layer, and so demonstrate the advantages of using FEA as a method to evaluate, design and understand SAW devices.

2. Simulation method

FEA using COMSOL multiphysics [7] facilitates computational modelling of the SAW as a resonant cavity which is perturbed from resonance upon application of layers at the sensor surface. These SAW devices in practice actually measure a $\Delta\varphi$ (phase change), not Δf frequency change, but one can be deduced from the other by the changes in acoustic wave velocity, Δv, upon layer addition. The perturbation that incurs a certain amount of Δv has been determined theoretically for some ideal materials [8], taking into account the application of a linear elastic mass, as:

$$\frac{\Delta f}{f} = \frac{\Delta v}{v} = \zeta \rho' h f \tag{1}$$

where ρ' is the added mass density and h is the height of the added mass, and the pertubative shift in frequency f is proportional by ζ (which depends on particular device parameters and can be experimentally verified) to the added linear elastic mass. Here we define the resonant mode as the mode that results in maximum average displacement over time. For any linear elastic mass addition we expect a change in frequency to be proportional to the change in added mass, i.e., the Sauerbrey equation (Eq. (1)) as derived for QCM [9] but more generally known as the perturbation formula for the SH-SAW [8,10]. It is, therefore, expected that by adding layers a decreasing shift in frequency will occur, and hence reduction in phase velocity.

The investigation described here uses FEA to solve the constitutive piezoelectric equations and find solutions for the displacements and electric potential (four degrees of freedom) incurred when an acoustic wave is induced at input IDTs. The resonant mode frequency, f, is defined by the maximum piezoelectric displacements. Determining Δf, and so Δv, upon adding biomarkers in a bioassay; it will be useful to compare the models to establish the expected linearity. This model can be used as a template for various other devices (other sensors can be simulated based on a template; important parameters that define the acoustic wave such

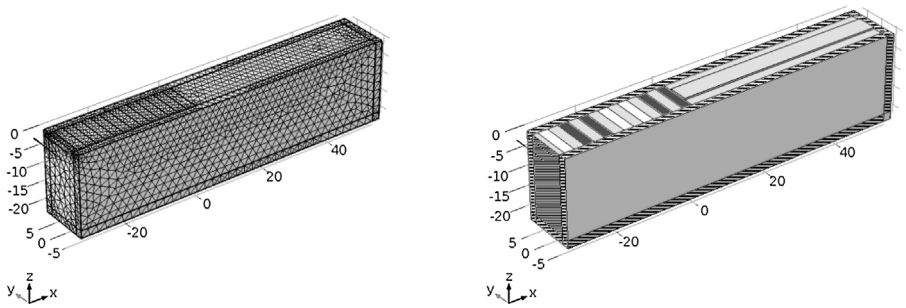

Fig. 2. Figure to show FEA model, units on the grid are μm; left-hand is the full view for the meshing displaying the finite elements distribution (surface is free triangular, remaining is tetrahedral). Input IDT electrodes are simulated using boundary conditions (are massless), a symmetry condition is also applied at the *zy* face (thin stripes) to reduce computational cost and effectively simulate 3 acoustic wavelengths of 20 μm. IDTS are indicated also in the right-hand diagram which displays the surface *xy* plane and the distribution of a gold "guiding" layer on the sensing area beyond the IDTs. Black regions indicate the positive applied potential, white indicate the negative applied potential. Boundaries along the edge of the device indicate a PML layer (thick stripes).

as device geometry, IDT periodicity, materials, crystal cut, can be easily adapted in FEA. However perhaps more importantly, it can be used as a characterized device to add 'biological layers' in order to predict the best surface chemistry for the most discriminate detection of disease biomarkers. These preliminary calculations examine the feasibility of the computational model as a tool for the design of biological layers in selective disease detection.

2.1. Mathematical method

The piezoelectric constitutive equations used are;

$$T_{ij} = c_{ijkl}S_{kl} - e_{kij}E_k \quad (2)$$

$$D_i = e_{ijk}S_{jk} + \epsilon_{ij}E_j \quad (3)$$

which couple the mechanical effect as governed by Newton's law and the electrical effect as determined by Gauss law, see references [11–13]. Where T_{ij} is the stress matrix, S_{jk} is the strain matrix, D_i is the electric displacement vector, E_j is the applied electric field vector and subscripts $i, j, k, l = x, y, z$. The material constants used as input are the elasticity (mechanical stiffness) matrix c_{ijkl}, the piezoelectric coupling matrix e_{ijk} and the permittivity matrix ϵ_{ij} (see Appendix A). In FEA the model is subdivided into small discrete elements which for acoustic wave problems require dimensions of at least $< \frac{\lambda}{5}$, where λ is the acoustic wavelength, to properly model the propagating wave.

2.2. FEA model

FEA was used to solve the above equations in 3-dimensions. The device design and geometry are shown in Fig. 2. Model parameters are displayed in Fig. 2 and Table 1. The device material is quartz with the cut 'poling' rotated about the *y*-axis, and so resonance is expected around 250 MHz, for its material and geometry, so frequency domain solutions are solved for around this operation frequency, with similar methodology to Ref. [14].

Input IDTs (2.5 μm width by 10 μm length) are defined by boundary conditions and arbitrary potentials are applied, +1 V and −1 V as indicated in Fig. 2, they are modelled as massless conductors for calculation simplification. Applying this external electric field generates a strain proportional to the applied field. The IDT SAW mode wavelength matches the IDT periodicity, acoustic wavelength 20 μm, and this λ is related by the dispersion relation to the SAW mode propagating velocity v and the resonant frequency f_0 as $v = \lambda_0 f_0$ [10]. Perfectly matched layers (PML's) are used to absorb the wave at the boundaries of the outer surfaces (in order to minimize reflection) [15]. Under investigation here is the effect of changing the crystal angle cut upon the nature of the acoustic waves launched. In this model *x* is taken to be the propagation direction, *y* is parallel to the SAW wavefront and *z* is normal to the surface, see Fig. 2. This model solves the piezo-electric constitutive equations in the stress-charge form (see elasticity matrix, coupling matrix and relative permittivity in Appendix A for the quartz material constants). In order to orient the material (*X*, *Y*, *Z*) to the coordinate system (*x*, *y*, *z*) and apply a 'cut'; a rotation matrix is applied (see Appendix A) to assign the appropriate 36-degree Y-cut quartz substrate (or '36Y-90X quartz') to the quartz material constants.

3. Results

3.1. The effect of crystal cut on the shear component of SAWs

This investigation searches for a mode with the largest displacement at the device surface; the mode that carries the sensing information. By definition, a SH-SAW has the main displacement component perpendicular to the direction of propagation and parallel to the surface. So when searching for a dominant SH-SAW mode in a particular cut we are searching for a dominant *y* component. This is analyzed in Fig. 3, which shows the absolute magnitude of *y* along the surface *xy* plane plotted against frequency for different angle rotations of the piezoelectric material, according to the rotation matrix defining the cut. Peaks on the graph indicate modes at frequencies with large shear components and the colour gradients in the right show the piezoelectric displacement (red for high, blue for low, the deformations are scaled for visibility) of these modes on the sensor surface.

Examining Fig. 3 and comparing the results for rotation angles of 36°y, 45° and 90° in particular – note there are no peaks for the 90° cut. At 90° there is virtually zero SH-SAW component observed, there is no resonant frequency in this range for this cut. In contrast

Table 1
Tables to show the model dimensions, geometry and boundary conditions used in FEA modelling.

Geometry	Value
Sensing length, *L*	52.5 μm
Pitch of electrodes, λ/2	10 μm
Width of electrode	2.5 μm
Length of electrode	10 μm
Height of sensor	20 μm
PML thickness	2 μm
Boundary	**Condition**
Fingers of IDT (black)	Electric potential 1 V
Alternate fingers IDT (white)	Electric potential −1 V
Remaining boundaries	Zero charge
Edge boundaries	PML scaled 20 μm
Symmetric plane	Symmetry

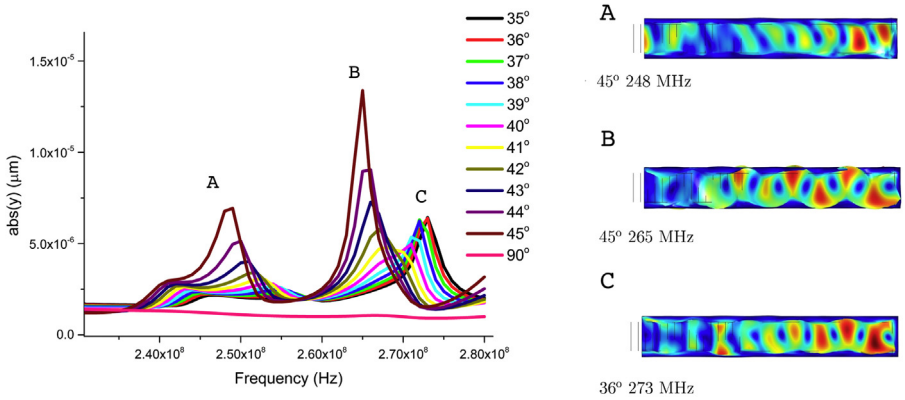

Fig. 3. Left: effect of crystal cut on SH-SAW mode, plotting the absolute value of displacement in the *y* direction against frequency for various rotations about *y*. Right: snapshots of the piezoelectric displacement along the surface for (A) 45° at 248 MHz, (B) 45° at 265 MHz and (C) 36° at 273 MHz.

the strongest peaks are observed in the 45° cut, peak A at 248 MHz and peak B, the largest peak, at 265 MHz, which demonstrates a periodic SH-SAW on the surface. Also shown is peak C, at 273 MHz, in the 36° cut. This deformation is also sinusoidal in character and similarly SH-SAW as in B.

3.2. Effect of adding gold to 36-degree Y-cut quartz substrates

The particular quartz device under investigation here has been optimized at 36° [16], where the piezoelectric is especially temperature stable, thus the following results focus on this cut and we examine the effect of adding a 0.4 μm layer of gold to the sensing surface in the model.

Examining Fig. 4 indicates that without gold, piezoelectric displacements appear SH-SAW-like at 273 MHz – there are large displacements in *y* – see peak C at 273 MHz and contrast E at 250 MHz where no SH-SAW appears. However, adding gold confines the wave to the surface and greatly enhances the displacements in *y*, which can be seen contrasting peak C with F and G in Fig. 4, and is in agreement with the general principle of Love wave generation [17]. The surface views demonstrate that adding a gold layer to the device surface causes a purer SH-SAW to propagate with sinusoidal character. Adding a layer of gold not only enhances displacements already present, contrast peak heights C and G in Fig. 4, but the resonant mode is also necessarily shifted by a reduction in *f* due to the added mass and also introduces new peaks of displacement, see F in Fig. 4. Note that upon adding gold a peak also appears at D, but the mode is not a pure SH-SAW as illustrated in F and G. F or G would appear to be an appropriate bio-sensing SH-SAW mode. As the displacements are enhanced upon the addition of a film layer, these results indicate a Love mode becomes the main mode of propagation [8] and demonstrates the guiding effect.

One advantage of the FEA analysis as demonstrated here is to enable observation of the wave in 3 dimensions. To examine the effect of the gold addition beyond the surface *xy* plane see Figs. 5 and 6, showing a cross-section view through the bulk of the model (*xz*). These figures show that adding the gold localizes the wave to the surface in contrast to the device with no gold – where we see piezoelectric displacements propagating in the bulk of the device. It can be seen directly that SSBWs are converted into SH-SAWs using a gold guiding layer.

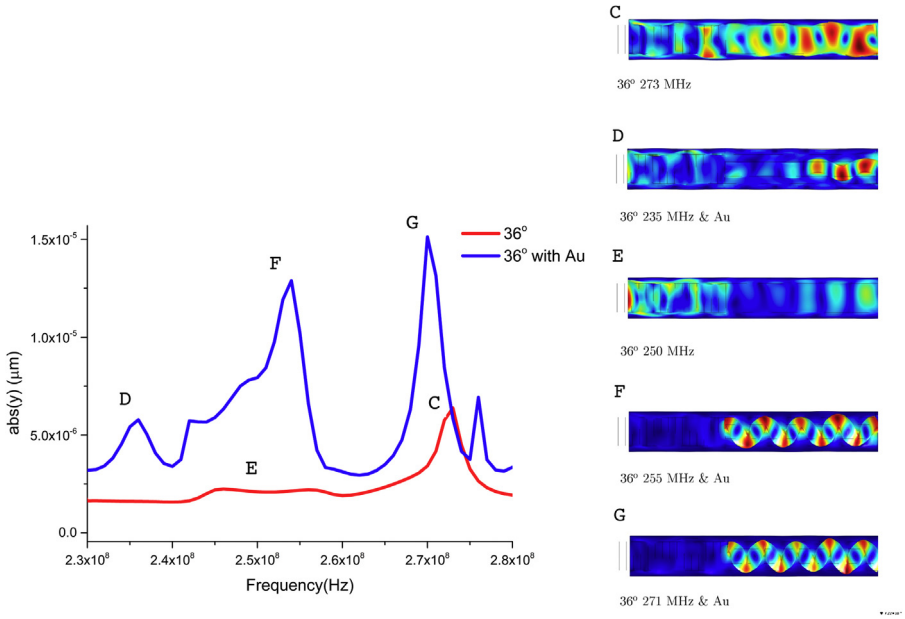

Fig. 4. Effect of gold layer added to surface of device, *xy* plane, plotting the absolute value of displacement in the *y* direction against frequency for 36°, with and without gold. Inset are snapshots for the surface piezoelectric displacement for various frequencies, C is 273 MHz (without gold), from Fig. 3, D is 235 MHz (with gold), E is 250 MHz (without gold), contrast these displacements with the pure SH-SAW shown in peaks (F) and (G) for the 36° with gold at 255 MHz and 271 MHz respectively.

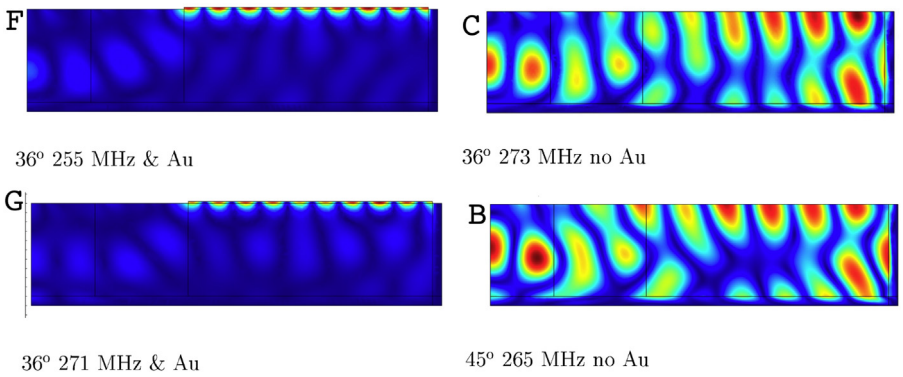

Fig. 5. Effect of gold layer added to surface of device, *xz* plane. Left are the results for 36° with gold at 255 MHz (top, F from Fig. 4) and 271 MHz (bottom, G from Fig. 4). Right are the results for 36° with no gold at 273 MHz (top, C from Figs. 3 and 4) and 45° with no gold at 265 MHz (bottom, B from Fig. 2) contrast the distributions of piezoelectric displacement for resonant modes with (left) and without (right) gold.

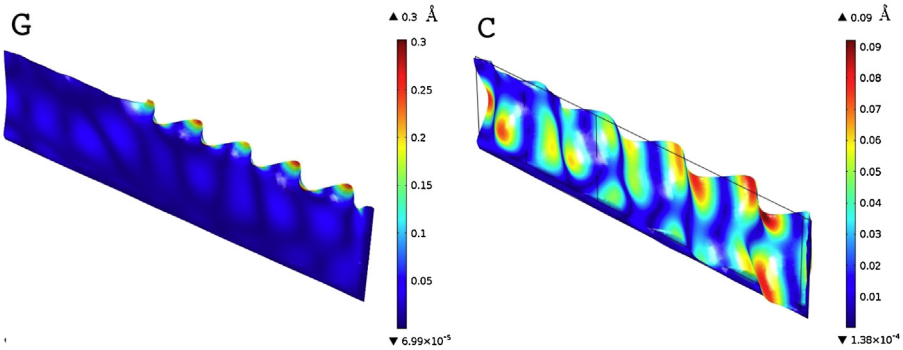

Fig. 6. 3D piezoelectric displacement for, left: (G) 36° with gold at 271 MHz (as in Fig. 5) and right: (C) 36° with no gold at 273 MHz (as in Fig. 5).

3.3. *Investigating different materials as guiding layers*

Above we have shown that the addition of a thin gold layer has the desirable effect of guiding the wave on the surface of the SAW sensor. In this next section we examine the effect of different materials on the guiding layer in order to optimize the sensitivity of this particular SAW chip. The requisite to create a guiding layer effect is to add a material with a low shear wave velocity [18] which must be less than in the device. Here we examine the effect of adding linear elastic materials of varying acoustic properties, see Table 2, on the piezoelectric displacement, the results are displayed in Fig. 7.

Fig. 7 shows the devices' response to adding 0.4 μm thick layers of gold, PMMA, titanium and platinum. These are all linear elastic materials of interest: gold is a common biosensor surface coating (it is stable and non-reactive), PMMA is a polymer also commonly used in SAW sensors as it is known to produce a guiding effect and interface well with biomaterial. Titanium and platinum where chosen due to their interesting acoustic properties for contrast – there is a relatively high shear velocity in titanium and relatively high acoustic impedance in platinum. Fig. 7 shows that comparing gold, PMMA, titanium and platinum within the frequency window of interest that platinum produces the largest shear displacements, see peak H at 243 MHz. Further the *xy* surface plot demonstrates a SH-SAW mode and the *xz* plane shows that the displacements are localized on the surface, similarly as in G, the guiding effect due to gold. In contrast PMMA shows a mode with shear displacement also, peak I at 248 MHz, but the *xz* plane demonstrates that the displacements progress through into the bulk. These results indicate that platinum may be a very good guiding material for SAW operation at 243 MHz, note however that gold produces a SH-SAW, G, with the added advantage of being bio- and sensor compatable.

It is shown here that a lower shear velocity is apparently not the only important acoustic property for the guiding layer, where it appears that PMMA (with the lowest shear velocity) does not eliminate bulk waves as well as gold or platinum. This result implies that a low shear velocity $V_s = \sqrt{\frac{C_{44}}{\rho}}$, where C_{44} is the shear

Table 2
Table of acoustic properties of materials used in this investigation, remaining are derived from the first three rows: the density, Young's modulus *E*, and Poisson's ratio.

Material property	Gold	PMMA	Titanium	Platinum
Young's modulus, *E* (GPa)	70	3	105	168
Density (kg/m^3)	19,300	1190	4940	21,450
Poisson's ratio	0.44	0.4	0.33	0.38
Shear velocity (m s^{-1})	1122	949	2827	1685
Shear modulus (GPa)	24.31	1.071	39.47	60.87
Bulk modulus, *K* (GPa)	194.4	5	102.9	233.3
Lame constant (GPa)	178.2	4.286	76.63	192.8
Acoustic impedance (MKS Rayls)	2.17e10^7	0.11e10^7	1.40e10^7	3.61e10^7

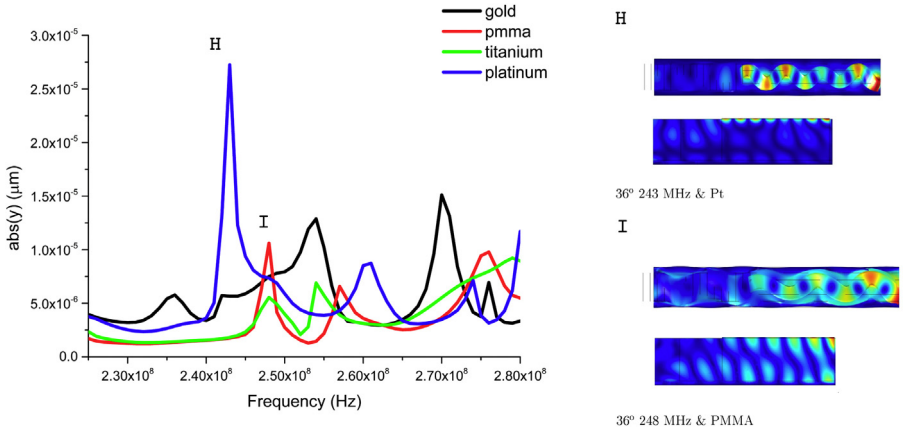

Fig. 7. Left: figure to demonstrate the effect of different materials on the piezoelectric displacement of the device, comparing 0.4 μm layers of gold, PMMA, titanium and platinum (see Table 2). A mode for platinum with comparably very large displacements labelled H, at 243 MHz, is displayed in the *xy* plane and the *xz* plane to show a guiding layer effect that compares to gold. Compare mode H in platinum with a mode in PMMA labelled I, at 248 MHz, which also exhibits shear displacements in the *xy* plane, but the *xz* plane shows propagation of the displacements into the bulk of the sensor). Platinum appears to be the 'best' at guiding.

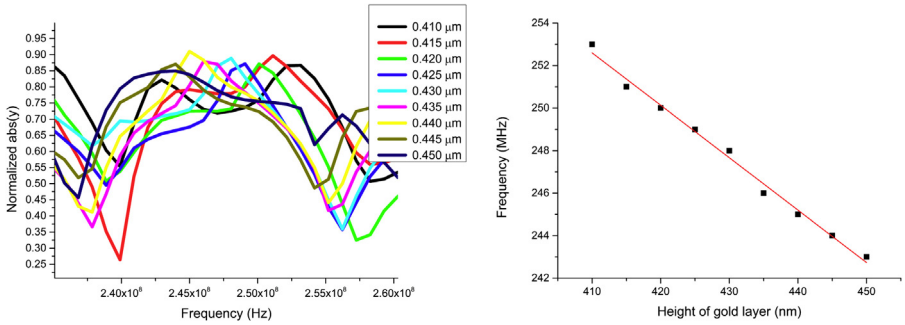

Fig. 8. Left: figure to show frequency shift with normalized displacements in the *y* direction for various thicknesses of added gold (0.410–0.450 μm) for the resonant mode around 250 MHz. Right: plot for the frequency peaks versus height of gold layer, demonstrating linearity, linear fit gives intercept 353.7 (standard error 3.6) MHz and slope −0.247 (standard error 0.008) MHz/nm.

modulus, combined with a high acoustic impedance $Z = \sqrt{C_{44}\rho}$ may be in combination more important given that gold and platinum show guiding effects.

3.4. Frequency shift with gold height

The relationship for shifting frequency with layer height can be easily computed using FEA, in thickness steps of 5 nm, and compared with the established theory, where the theoretical expression for adding mass layers to quartz resonators is as in Eq. (1). In this result the normalized particle displacements of the *y*-component, $\frac{|y|}{|x|+|y|+|z|}$, indicates the mode with the largest relative shear component (and least bulk wave loss), see Fig. 8, which demonstrates the relationship and validates the model.

3.5. Discussion

This investigation indicates a calibration with Eq. (1) [10], The Sauerbrey equation, and proves the validity of our model. This is an important step towards developing models for the device for fluid perturbations and, more complicated, biolayer applications. The theoretical relationship between viscosity effects and changes to the acoustic wave has been determined for SH-SAW quartz devices before: this is derived from analysis of the perturbations affecting the complex surface mechanical impedance [19,20]. It has been previously determined that the largest perturbations to the wave, for this device type, appear to come from viscosity changes on the surface [16], the viscosity having a greater effect than mass [1]. Pertinent towards the next steps in this line of work would be to compare the fluid effects for this model to those resulting from an FEA model based on the one outlined here, as well as comparison with experiment. Beyond determination of simpler viscous effects (such as glycerol) if there is good experimental agreement the model will be determined robust enough for considering the effect of bio-matter, where the visco-elastic relationship may not be straightforward. Surface acoustic (elastic) waves and the theory of the physics that define them is greatly simplified when the material is infinite, homogeneous, elastic, isotropic and a solid. Typical biological layers do not typically possess these attributes. For example to define a soft layer we can assume Lamé constants (both) ~1.0 GPa, density 1000 kg/m^3 and relative permittivity 1 [8], the advantage of FEA is that a range of these parameters can be readily explored to find a combination of those properties that produce the most perturbative affect. Biological layers will typically have a low shear modulus, but how exactly the cross-linking in biomolecules may effect the shear modulus and how releasing molecules in reactions may decrease surface mass density are all objects of interest to be quantified and will have to be explored in the determination of this SH-SAW device for particular biomarkers in disease detection. Given that sensing occurs in the bio-layer within which there must be ample displacements, so as the wave in the device couples with waves in the biolayer sample, biomolecular interactions need to take place within the penetration depth [21]. A penetration depth of $\delta = 66$ nm is predicted from $\delta = \sqrt{\frac{\eta}{\pi f \rho_{sol}}}$,

using an operating frequency $f = 250$ MHz, and an approximate density $\rho_{sol} = 1025$ kg/m^3 and dynamic viscosity $\eta = 0.0035$ Pa s for blood. Therefore detection of antibodies (~110 nm), small proteins (~15 nm) and DNA (~12 nm) in blood samples should be entirely feasible using a biosensing mode, such as that seen in G see Fig. 4, as found in this investigation.

4. Conclusions

It has been shown that 3D FEA is a particularly useful tool for examining the piezoelectric displacements launched in all directions without the usual reduction to 2 dimensions, as is usually tacitly assumed for pure SH-SAW waves. A 3D model allows wider investigation of the nature of the launched wave with respect to device parameters (cut, geometry, material constants). Dominant displacements at a range of quartz cuts were investigated and it was shown that at a 36-degree Y-cut, with the addition of gold, the wave is guided into a SH-SAW; cross sectional figures show the gold layer concentrates the propagation of the wave into the surface. This energy trapping effect that increases surface sensitivity [17,22], is the acoustic analogue of the "skin effect" observed when a material layer is added to a conductor excited by an alternating electric current [23]. The surface figures show the main displacement (the polarization) is perpendicular to the propagation direction: the surface waves are shear. This is in agreement to what is believed to be the case for these particular sensor designs. It should be noted also that a 45° cut looks promising with respect to generating SH-SAW's, and again demonstrates the utility of this FEA analysis as a tool for optimizing sensor design and easily and cheaply probing new chip geometries, cuts and materials. Bulk material properties, such as used here, may not always recreate truly the physical effects that exist on the sub-micron scale (i.e., very thin films), however with the agreement to the perturbation formula demonstrated here, it is shown that elastic properties at this scale (sub-micron films) reproduce the expected results, though note not all bulk properties, such as hardness, as in Ref. [24] may. Also examined here is the effect of different materials as guiding layers: the stipulation of a lower acoustic velocity doesn't seem to be the only criterion for creation of a sensitive propagating SH-SAW, but also a high acoustic impedance is advantageous. Investigation into platinum as an effective guiding layer would have merit with respect to enhanced sensing. Lastly it has been shown that adding a linear elastic mass such as gold results in a guiding layer effect, where the change in frequency is proportional to the added mass, as predicted by the Sauerbrey equation, thus establishing the model as reliable for a "baseline" signal and suitable for next stage solutions involving biomolecular markers in fluids.

Acknowledgements

We would like to thank Dr Dale Athey and Dr Hiromi Yatsuda from OJ-Bio and Japan Radio Company, Ltd. Valérian Turbé and Mike Goto for discussions. For funding we would like to gratefully acknowledge the EPSRC i-sense IRC in Early Warning Sensing Systems for Infectious Diseases reference EP/K031953/1 and the NIHR i4i award for Next Generation Mobile Diagnostics for HIV with Wireless Connectivity.This article presents independent research funded by the National Institute for Health Research (NIHR) under the project code II-LA-1111-20004 Next Generation Mobile HIV Diagnostics with Wireless Connectivity. The views expressed are those of the authors and not necessarily those of the NHS, the NIHR or the Department of Health. Thanks to the Royal Society for Wolfson Research Merit Award (Rachel McKendry).

Appendix A. Material constants

Quartz material constants input into COMSOL (stress-charge form):

$$c_{IJ}[\times 10^{11}\,\mathrm{N/m^2}] = \begin{bmatrix} 0.867362 & 0.0698527 & 0.119104 & 0.179081 & 0 & 0 \\ 0.0698527 & 0.867362 & 0.119104 & -0.179081 & 0 & 0 \\ 0.119104 & 0.119104 & 1.07194 & 0 & 0 & 0 \\ 0.179081 & -0.179081 & 0 & 0.579428 & 0 & 0 \\ 0 & 0 & 0 & 0 & 0.579492 & 0.179224 \\ 0 & 0 & 0 & 0 & 0.179224 & 0.399073 \end{bmatrix}$$

Coupling matrix:

$$e_{IJ}[\mathrm{C/m^2}] = \begin{bmatrix} -0.19543 & 0.19543 & 0 & -0.12120 & 0 & 0 \\ 0 & 0 & 0 & 0 & 0.12127 & 0.19558 \\ 0 & 0 & 0 & 0 & 0 & 0 \end{bmatrix}$$

Relative permitivity:

$$\epsilon_{ij}[\times 10^{11}\,\mathrm{F/m}] = \begin{bmatrix} 4.4093 & 0 & 0 \\ 0 & 4.4092 & 0 \\ 0 & 0 & 4.68 \end{bmatrix}$$

These material constants are based on the 1978 IEEE LH convention.

Rotation matrix applied for a 36-degree Y-cut crystal orientation:

$$\begin{bmatrix} 0 & 1 & 0 \\ \sin((36/180)*pi)) & 0 & \cos((36/180)*pi \\ \cos((36/180)*pi) & 0 & -\sin((36/180)*pi) \end{bmatrix}$$

References

[1] H. Yatsuda, T. Kogai, M. Goto, N. Yoshimura, Shear-horizontal surface acoustic wave biosensors for POCT, in: 2014 IEEE International Frequency Control Symposium (FCS), 2014, pp. 1–4.
[2] S. Shiokawa, J. Kondoh, Surface acoustic wave sensors, Jpn. J. Appl. Phys. 43 (5S) (2004) 2799 http://iopscience.iop.org/1347-4065/43/5S/2799.
[3] J. Kondoh, Y. Okiyama, S. Mikuni, Y. Matsui, M. Nara, T. Mori, H. Yatsuda, Development of a shear horizontal surface acoustic wave sensor system for liquids with a floating electrode unidirectional transducer, Jpn. J. Appl. Phys. 47 (5S) (2008) 4065 http://iopscience.iop.org/1347-4065/47/5S/4065.
[4] F. Bender, R.E. Mohler, A.J. Ricco, F. Josse, Identification and quantification of aqueous aromatic hydrocarbons using SH-surface acoustic wave sensors, Anal. Chem. (2014), http://dx.doi.org/10.1021/ac403724f.
[5] C. Campbell, Surface Acoustic Wave Devices for Mobile and Wireless Communications, Academic Press, 1998.
[6] F. Bender, K. Lange, N. Barie, J. Kondoh, M. Rapp, On-line monitoring of polymer deposition for tailoring the waveguide characteristics of love-wave biosensors, Langmuir 20 (6) (2004) 2315–2319.
[7] [COMSOL 4.4 Multiphysics. http://www.comsol.com/release/4.4.
[8] J. Kondoh, Theoretical consideration of high-sensitivity biosensor using shear horizontal acoustic waves in layered structures, Electron. Commun. Jpn. 95 (4) (2012) 27–32, http://dx.doi.org/10.1002/ecj.10417/abstract.
[9] A. Pomorska, D. Shchukin, R. Hammond, M.a. Cooper, G. Grundmeier, D. Johannsmann, Positive frequency shifts observed upon adsorbing micron-sized solid objects to a quartz crystal microbalance from the liquid phase, Anal. Chem. 82 (6) (2010) 2237–2242.
[10] D.S. Ballantine, R.M. White, S.J. Martin, A.J. Ricco, E.T. Zellers, G.C. Frye, H. Wohltjen, Acoustic Wave Sensors, Theory, Design, and Physico-Chemical Applications, Academic Press, 1997.
[11] B. Auld, Acoustic Fields and Waves in Solids, vols. I and II, John Wiley and Sons, 1973.
[12] N. Botkin, M. Schlensog, M. Tewes, V. Turova, A mathematical model of a biosensor, Model. Simulat. Microsyst. (2001) 231–234.
[13] P. Wang, J. Su, L. Gong, M. Shen, M. Ruths, H. Sun, Numerical simulation and experimental study of resonance characteristics of QCM-P devices operating in liquid and their application in biological detection, Sens. Actuators B: Chem. 220 (2015) 1320–1327 http://www.sciencedirect.com/science/article/pii/S0925400515300812.
[14] A.A. Mohanan, M.S. Islam, S.H. Ali, R. Parthiban, N. Ramakrishnan, Investigation into mass loading sensitivity of sezawa wave mode-based

surface acoustic wave sensors, Sensors (Basel, Switzerland) 13 (2) (2013) 2164–2175 http://www.mdpi.com/1424-8220/13/2/2164/htm.
[15] Y. Li, O. Bou Matar, Convolutional perfectly matched layer for elastic second-order wave equation, J. Acoust. Soc. Am. 127 (3) (2010) 1318–1327 http://scitation.aip.org/content/asa/journal/jasa/127/3/10.1121/1.3290999.
[16] M. Goto, H. Yatsuda, J. Kondoh, Analysis of mass loading effect on guided shear horizontal surface acoustic wave on liquid/au/quartz structure for biosensor application, Jpn. J. Appl. Phys. 52 (7S) (2013) 07HD10 http://adsabs.harvard.edu/abs/2013JaJAP.52gHD10G.
[17] W. Wang, S. He, Theoretical analysis on response mechanism of polymer-coated chemical sensor based Love wave in viscoelastic media, Sens. Actuators B: Chem. 138 (2) (2009) 432–440 http://www.sciencedirect.com/science/article/pii/S0925400509002032.
[18] Z. Wang, J. Cheeke, C.K. Jen, Sensitivity analysis for love mode acoustic gravimetric sensors, Appl. Phys. Lett. 64 (22) (1994) 2940–2942.
[19] J. Kondoh, S. Shiokawa, M. Rapp, S. Stier, Simulation of viscoelastic effects of polymer coatings on surface acoustic wave gas sensor under consideration of film thickness, Jpn. J. Appl. Phys. 37 (5S) (1998) 2842, URL http://iopscience.iop.org/1347-4065/37/5S/2842.
[20] K. Mitsakakis, A. Tsortos, J. Kondoh, E. Gizeli, Parametric study of SH-SAW device response to various types of surface perturbations, Sens. Actuators B: Chem. 138 (2) (2009) 408–416 http://www.sciencedirect.com/science/article/pii/S0925400509001683.
[21] K. Saha, F. Bender, A. Rasmusson, E. Gizeli, Probing the viscoelasticity and mass of a surface-bound protein layer with an acoustic waveguide device, Langmuir 19 (4) (2003) 1304–1311.
[22] E. Gizeli, N.J. Goddard, C.R. Lowe, A.C. Stevenson, A Love plate biosensor utilising a polymer layer, Sens. Actuators B: Chem. 6 (1–3) (1992) 131–137.
[23] G. Sposito, P. Cawley, P.B. Nagy, An approximate model for three-dimensional alternating current potential drop analyses using a commercial finite element code, NDT&E Int. 43 (2) (2010) 134–140 http://www.sciencedirect.com/science/article/pii/S0963869509001492.
[24] W.D. Nix, Mechanical properties of thin films, Metall. Trans. A 20 (11) (1989) 2217–2245.